Trends in Organic Chemistry
Vol. 16, 2012

Original Communication

A computational study of the thermal *cis*-to-*trans* isomerization of N-(phenylazo)-substituted nitrogen heterocycles

Jinlong Fu and Mónica Barra*

Department of Chemistry, University of Waterloo, 200 University Avenue West, Waterloo, Ontario N2L 3G1, Canada

ABSTRACT

The structure and relative stability of ground-state isomeric forms and corresponding transition states for thermal *cis*-to-*trans* isomerization of a series of N-(phenylazo)-substituted nitrogen heterocycles were calculated, in cyclohexane and dimethylsulfoxide, using density functional theory combined with the polarizable continuum solvation model. Bond length trends and solvent-induced geometry changes are rationalized in terms of the degree of π-donation from N-heterocycle to phenylazo moiety. Isomerization is predicted to proceed by a rotation mechanism via a zwitterionic transition state structure. Computed Gibbs energies of activation reproduce qualitatively experimental reactivity trends previously reported; resulting rate constants, however, are ca. 2 to 57 times higher than corresponding experimental values.

KEYWORDS: photochromism, triazenes, *Z-E* isomerization, DFT study, PCM model

INTRODUCTION

The study of unsaturated compounds able to undergo reversible changes in double-bond configuration upon exposure to light continues to be an active area of research owing to the utility of these materials in the design, for example, of biosensors, molecular motors and shuttles, high-density data storage media and switching elements for microelectronics [1]. An interesting class of photoswitchable material based on *cis-trans* isomerization around a nitrogen-nitrogen double bond is represented by triazenes, compounds that have a diazoamino (triazeno) moiety (–N=N–N<) and offer potential use in light-driven molecular switches [2].

Recent studies from our laboratory have focused on the mechanism of the thermal *cis*-to-*trans* isomerization of trisubstituted triazenes, using N-(phenylazo)-substituted nitrogen heterocycles as substrates (Chart 1). *Cis* forms were generated upon UV-lamp irradiation of corresponding *trans* isomers either dissolved in organic solvents [3] or incorporated in doped polymer films [4]. Rate constants for thermally driven *cis*-to-*trans* isomerization were found to increase as the electron-withdrawing character of the phenyl ring substituent, the N-heterocycle ring size, and the polarity of the reaction medium increased as well [3, 4]. These experimental findings were interpreted in terms of an internal rotation mechanism involving heterolytic rupture of the nitrogen-nitrogen π-bond and out of plane torsion around the C-N=N-N dihedral angle, as illustrated in Scheme 1. Such a pathway is analogous to the rotational mechanism characteristic of 'push-pull' (donor/acceptor-substituted) azobenzenes [5].

The relationship between structure (i.e., phenyl substituent, N-heterocycle), reaction medium and

*Corresponding author
mbarra@uwaterloo.ca

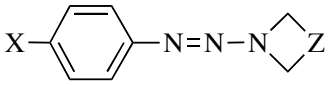

Substrate	X	Z
X-4	CH_3O, H, Cl, CF_3	CH_2
X-5	CH_3O, CH_3, H, CF_3	$(CH_2)_2$
X-6	CH_3O, H	$(CH_2)_3$
X-6O	CH_3O, H	CH_2OCH_2
X-7	CH_3O, H	$(CH_2)_4$

Chart 1. Structure and abbreviation of compounds studied.

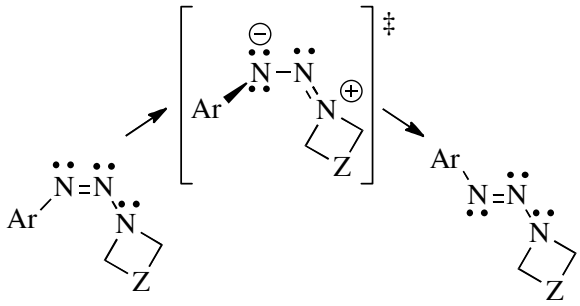

Scheme 1

isomerization rate is of fundamental importance to control and exploit 1-phenyltriazenes as photo-responsive materials. The set of experimental rate constants available for thermal *cis*-to-*trans* isomerization, however, is somewhat limited, partly due to (photoinduced) decomposition taking place under certain conditions or isomerization being too fast to be measured with our system [3]. Theoretical studies can certainly aid at determining whether the trends inferred from (a limited set of) experimental isomerization rate values would indeed hold for all target substrates. Preliminary DFT calculations, performed at the B3LYP/6-31G(d) level, for gas phase isomerization of substrates listed in Chart 1 support indeed a rotation mechanism [3]. Potential energy curves calculated for gas-phase isomerization of H-5, for instance, show that the energy barrier for isomerization via rotation around the N=N group is lower than that for isomerization via a transition state involving an sp hybridized azo-nitrogen atom (i.e., an inversion mechanism, as in the case of azobenzene [5]). Moreover, calculated gas phase energy barriers are found to diminish as the electron-withdrawing character of the phenyl ring substituent and the N-heterocycle ring size also increase [3]. The theoretical study presented herein is a continuation of the earlier work on in vacuo simulations, and aimed at investigating solvent effects on the geometry and relative stability of ground-state isomeric forms of substrates listed in Chart 1, and of corresponding transition states for thermal *cis*-to-*trans* isomerization. Correlations between calculated Gibbs energies of activation and reported experimental rate constants are presented as well.

EXPERIMENTAL

Computational methodology

All structures were fully optimized using the DFT-B3LYP method and 6-31G(d) basis set, combined with the IEF-PCM solvation model as implemented in the Gaussian 09 package of programs [6]; transition states were located by using the synchronous transit-guided quasi Newton method (QST2 and QST3) options. Vibrational frequency calculations were carried out in all cases to confirm the stationary points as either minima or first-order saddle points, and to obtain Gibbs energy values at 294.15 K.

RESULTS AND DISCUSSION

Optimized geometries for *cis* and *trans* isomers and for transition state (*TS*) structures were calculated in cyclohexane (CH) and dimethyl-sulfoxide (DMSO) using the integral equation formalism (IEF) version of the polarizable continuum solvation model (PCM) [7]. Selected geometric parameters and relative energies for computed structures are summarized in Tables 1 and 2. As shown in Figure 1 for H-6O as an example, the planar phenyl ring in the optimized *cis* isomers, unlike in the *trans* forms, is rotated out of the plane of the triazeno moiety due to steric repulsions with the N-heterocycle. Accordingly, as listed in Tables 1 and 2, the energy difference between ground-state isomeric forms is found to increase with increasing N-heterocycle ring size.

Comparison of bond lengths listed in Tables 1 and 2 for ground-state *cis* and *trans* isomers shows that, for any given substrate, the N=N bond length

Table 1. Selected bond lengths, bond angles, dihedral angles, dipole moments, and relative potential energies computed in cyclohexane using DFT-B3LYP/6-31G(d) method and IEF-PCM model.

Parameter	*Cis*	*TS*[a]	*trans*	*cis*	*TS*[a]	*trans*	*cis*	*TS*[a]	*trans*
	CH_3O-4			**CH_3O-5**			**CH_3O-6**		
N=N (pm)	125.9	127.9	126.8	126.0	128.2	127.5	125.5	127.6	126.7
N–N (pm)	135.9	130.4	133.5	136.5	130.8	132.0	139.2	132.0	134.3
C–N=N (deg)	124.5	133.5	114.2	126.0	132.3	113.7	126.6	132.5	113.9
N=N–N (deg)	122.3	115.3	113.2	123.0	115.7	114.0	122.8	118.0	115.4
C-N=N-N (deg)	-7.7	-89.8	-177.2	11.5	91.7	-179.7	8.7	89.4	175.6
Dipole (D)	4.14	6.09	2.03	4.00	6.33	2.71	3.76	5.79	1.90
ΔE^b (kcal mol^{-1})		24.3	-11.3		20.3	-14.6		18.7	-16.4
	CH_3O-6O			**CH_3O-7**			**CH_3-5**		
N=N (pm)	125.3	127.1	126.5	126.1	127.6	127.1	126.0	128.3	127.6
N–N (pm)	140.0	132.5	134.7	136.4	131.8	133.3	135.8	130.6	131.7
C–N=N (deg)	126.8	134.0	114.1	126.7	134.4	113.9	126.0	132.2	113.6
N=N–N (deg)	122.4	117.6	114.8	124.9	117.3	114.8	123.3	115.7	114.0
C-N=N-N (deg)	8.3	89.4	175.6	-10.8	-88.8	-176.0	11.9	91.7	-179.7
Dipole (D)	3.24	5.09	0.85	4.44	5.76	2.08	4.29	6.92	3.31
ΔE^b (kcal mol^{-1})		19.6	-16.2		18.6	-16.9		18.7	-14.3
	H-4			**H-5**			**H-6**		
N=N (pm)	126.0	128.1	126.9	126.0	128.3	127.6	125.6	127.6	126.9
N–N (pm)	135.1	130.1	132.8	135.5	130.5	131.6	137.3	131.7	133.7
C–N=N (deg)	124.2	133.3	114.0	126.0	132.2	113.6	126.3	132.9	113.7
N=N–N (deg)	122.5	115.3	113.3	123.3	115.8	114.0	123.9	118.1	115.5
C-N=N-N (deg)	7.8	89.5	176.9	12.3	91.7	-179.6	9.3	89.0	175.7
Dipole (D)	4.26	6.90	2.89	4.32	7.14	3.80	4.00	6.74	3.01
ΔE^b (kcal mol^{-1})		21.8	-11.0		17.9	-14.3		16.1	-16.3
	H-6O			**H-7**			**Cl-4**		
N=N (pm)	125.4	127.2	127.0	126.1	127.7	127.2	126.1	128.6	127.1
N–N (pm)	138.0	132.2	133.4	135.7	131.5	132.9	134.7	129.5	132.4
C–N=N (deg)	126.2	134.1	113.6	126.8	134.3	113.6	124.3	131.7	113.8
N=N–N (deg)	123.4	117.7	115.3	125.2	117.3	114.8	122.6	115.3	113.3
C-N=N-N (deg)	8.6	89.2	175.1	-11.1	-88.6	-175.8	8.3	89.3	177.1
Dipole (D)	2.58	4.86	1.38	3.90	6.55	3.05	4.36	9.29	5.39
ΔE^b (kcal mol^{-1})		17.1	-16.0		16.4	-16.5		20.8	-11.4
	CF_3-4			**CF_3-5**					
N=N (pm)	126.1	128.8	127.4	126.2	128.8	127.9			
N–N (pm)	134.2	129.1	131.8	134.7	129.8	131.0			
C–N=N (deg)	124.3	131.5	113.6	126.2	131.3	113.3			
N=N–N (deg)	122.6	115.4	113.4	123.4	115.9	114.1			
C-N=N-N (deg)	8.8	89.3	177.1	14.1	91.0	-179.6			
Dipole (D)	4.94	10.49	6.59	5.46	10.68	7.46			
ΔE^b (kcal mol^{-1})		18.7	-11.4		14.9	-14.8			

[a]Transition state structure. [b]Relative to *cis* isomeric form; ZPE correction included.

Table 2. Selected bond lengths, bond angles, dihedral angles, dipole moments, and relative potential energies computed in dimethylsulfoxide using DFT-B3LYP/6-31G(d) method and IEF-PCM model.

Parameter	*Cis*	*TS*[a]	*trans*	*cis*	*TS*[a]	*trans*	*cis*	*TS*[a]	*trans*
	CH_3O-4			**CH_3O-5**			**CH_3O-6**		
N=N (pm)	126.4	130.1	127.1	126.5	130.0	127.8	126.0	129.2	127.0
N–N (pm)	134.9	128.3	132.9	135.2	129.1	131.5	137.4	130.4	133.7
C–N=N (deg)	124.3	127.6	114.2	125.7	127.9	113.6	126.4	128.6	113.8
N=N–N (deg)	122.8	115.6	113.5	123.6	116.1	114.4	123.8	118.3	115.7
C-N=N-N (deg)	-7.8	-90.0	-177.1	12.2	91.8	-179.7	9.5	89.2	175.4
Dipole (D)	4.92	7.72	2.44	4.83	7.77	3.22	4.55	7.28	2.36
ΔE^b (kcal mol^{-1})		23.0	-10.6		19.1	-14.0		17.5	-15.8
	CH_3O-6O			**CH_3O-7**			**CH_3-5**		
N=N (pm)	125.7	128.7	126.8	126.5	129.2	127.4	126.6	129.9	127.9
N–N (pm)	138.7	130.9	134.1	135.4	130.3	132.8	134.6	129.0	131.2
C–N=N (deg)	126.7	129.7	113.9	126.7	129.8	113.7	125.9	128.3	113.5
N=N–N (deg)	123.2	117.9	115.2	125.5	117.7	115.1	123.9	116.1	114.4
C-N=N-N (deg)	8.8	89.5	175.3	-11.1	-88.6	-175.9	12.4	91.6	-179.5
Dipole (D)	3.69	5.14	0.87	5.55	7.24	2.64	5.24	8.46	3.90
ΔE^b (kcal mol^{-1})		18.6	-15.5		17.8	-16.0		17.5	-13.8
	H-4			**H-5**			**H-6**		
N=N (pm)	126.4	130.2	127.3	126.6	130.0	128.0	126.2	129.3	127.2
N–N (pm)	134.0	128.0	132.1	134.3	128.9	131.0	135.6	130.1	133.0
C–N=N (deg)	124.0	127.7	113.8	125.9	128.2	113.4	126.4	129.0	113.5
N=N–N (deg)	122.9	115.5	113.6	123.9	116.1	114.4	125.0	118.5	115.8
C-N=N-N (deg)	8.0	89.8	176.9	12.8	91.5	-179.5	9.9	88.8	175.4
Dipole (D)	5.11	8.73	3.54	5.24	8.77	4.49	4.94	8.41	3.67
ΔE^b (kcal mol^{-1})		20.3	-10.3		16.6	-13.8		15.5	-15.6
	H-6O			**H-7**			**Cl-4**		
N=N (pm)	125.8	128.7	127.0	126.5	129.3	127.6	126.6	130.6	127.6
N–N (pm)	136.7	130.7	133.4	134.8	130.0	132.3	133.6	127.7	131.5
C–N=N (deg)	126.3	130.7	113.6	126.7	130.0	113.5	124.1	126.9	113.6
N=N–N (deg)	124.3	118.2	115.3	125.6	117.7	115.2	123.1	115.6	113.7
C-N=N-N (deg)	8.9	88.9	175.1	-11.5	-88.4	-175.7	8.6	89.5	177.1
Dipole (D)	3.16	6.25	1.63	4.02	8.23	3.78	5.22	11.23	6.44
ΔE^b (kcal mol^{-1})		16.0	-15.3		15.5	-15.7		19.0	-10.6
	CF_3-4			**CF_3-5**					
N=N (pm)	126.6	130.7	127.9	126.8	130.4	128.3			
N–N (pm)	133.2	127.4	130.9	133.6	128.4	130.5			
C–N=N (deg)	124.2	126.9	113.4	126.1	127.7	113.1			
N=N–N (deg)	123.0	115.7	113.7	123.9	116.2	114.4			
C-N=N-N (deg)	9.3	89.4	177.2	15.0	90.8	-179.4			
Dipole (D)	5.81	12.45	7.75	6.39	12.54	8.49			
ΔE^b (kcal mol^{-1})		16.8	-10.6		13.3	-14.2			

[a]Transition state structure. [b]Relative to *cis* isomeric form; ZPE correction included.

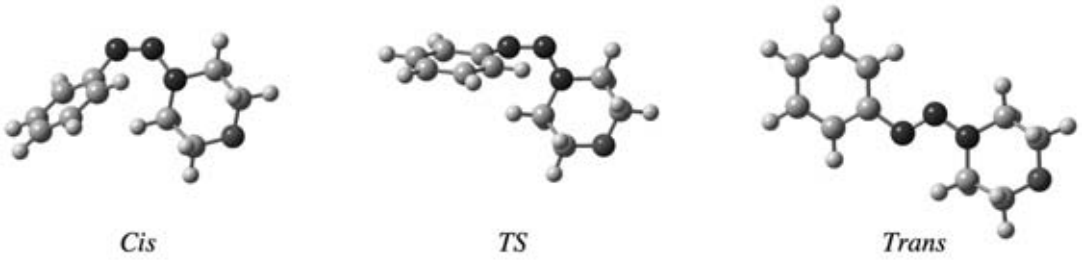

Figure 1. Computed structures for H-6O in cyclohexane using IEF-PCM model.

increases in the order *cis* < *trans* while the N–N distance decreases in the order *cis* > *trans*. Also, for any given *cis* or *trans* form, lengthening of the N=N bond accompanied by shortening of the N–N bond is evident when comparing CH values with those computed in DMSO; similar trends result as well when comparing reported values for gas phase [3] with those listed in Table 1 for CH. Moreover, for any given N-heterocycle, an increase in the N=N bond length and decrease in the N–N distance is noticed in *trans* isomers, as the electron-withdrawing character of the phenyl X substituent increases. Since, to the best of our knowledge, X-ray data for target triazenes are not available, it is worthy to note here that DFT-B3LYP/6-31G(d) geometric parameters obtained for *trans*-(2,6-*cis*-dimethyl-N-phenylazo)-piperidine are in excellent agreement with X-ray data [8]. All the observations just described can be explained by writing the following two resonance structures for the triazeno moiety: $-N^{(1)}=N^{(2)}-N^{(3)}< \leftrightarrow -N^{-}-N=N^{+}<$. As π-conjugation (with phenyl ring at $N^{(1)}$) and solvent polarity increase so does the stability (and hence, contribution) of the dipolar resonance form, thus leading to a decrease and an increase in $N^{(1)}=N^{(2)}$ and $N^{(2)}-N^{(3)}$ bond distances, respectively, on going from *cis* to *trans* and from CH to DMSO. It should be pointed out here that computed solvent-induced geometry changes for 'push-pull' (donor/acceptor) π-conjugated molecules are not unprecedented [9].

The trends in bond lengths described above for the triazeno moiety in ground-state isomeric forms, and their rationalization in simple terms based on the contribution of a dipolar canonical form, are consistent with the electron charge distributions obtained via the natural population analysis (NPA). As summarized in Table 3, the negative charge on $N^{(1)}$ increases and that on $N^{(3)}$ decreases, for any given substrate, on going from *cis* to *trans* and from CH to DMSO (i.e., as the influence of the dipolar resonance form increases).

As illustrated in Figure 1 as well for H-6O, the optimized transition state structures for thermal *cis*-to-*trans* isomerization reveal rotation around the N=N bond. In addition to torsion around the C-N=N-N dihedral angle, comparison of values listed in Tables 1 to 3, for any given substrate on going from *cis* to *TS*, shows (i) lengthening of the N=N bond, (ii) shortening of the N–N bond, (iii) substantial increase in molecular dipole moment, (iv) increase in $N^{(1)}$ negative charge, and (v) decrease in $N^{(3)}$ negative charge. All these trends are certainly indicative of isomerization involving heterolytic cleavage of, and torsion around, the N=N π-bond.

Gibbs energies of activation ($\Delta G^{\ddagger} = G_{TS} - G_{cis}$) for thermal *cis*-to-*trans* isomerization computed in CH and DMSO, as well as in gas phase, are depicted in Figures 2 and 3. Clearly, for any given substrate, $\Delta G^{\ddagger}$ diminishes in the order gas phase > CH > DMSO (i.e., as the dielectric constant of the reaction medium increases), consistent with the solvent effect predicted based on the Hughes-Ingold rules for a system involving separation of charges at the activated complex [10], as in the case of Scheme 1. Figure 2 also illustrates the dependence of $\Delta G^{\ddagger}$ on phenyl substituent; for any given reaction medium, $\Delta G^{\ddagger}$ diminishes with increasing electron-withdrawing character of the X group. Such a dependency is rationalized in terms of the ability of the phenyl ring to stabilize the negative charge that develops on $N^{(1)}$ at the zwitterionic *TS* structure. In fact, inspection of corresponding molecular orbital levels shows that electron-withdrawing groups stabilize the HOMO

Table 3. NPA charges (q_N, in a. u.) in triazeno moiety ($-N^{(1)}=N^{(2)}-N^{(3)}<$) computed in cyclohexane and dimethylsulfoxide using DFT-B3LYP/6-31G(d) method and IEF-PCM model[a].

Substrate	$q_{N(1)}$			$q_{N(2)}$			$q_{N(3)}$		
	cis	*TS*[b]	*trans*	*cis*	*TS*[b]	*trans*	*cis*	*TS*[b]	*trans*
CH_3O-4	-0.243	-0.358	-0.301	0.007	0.092	-0.019	-0.309	-0.179	-0.254
	(-0.271)	(-0.415)	(-0.319)	(-0.003)	(0.092)	(-0.022)	(-0.297)	(-0.134)	(-0.248)
CH_3O-5	-0.251	-0.371	-0.333	0.003	0.084	-0.020	-0.294	-0.164	-0.224
	(-0.282)	(-0.416)	(-0.352)	(-0.006)	(0.081)	(-0.023)	(-0.276)	(-0.125)	(-0.212)
CH_3O-6	-0.221	-0.362	-0.313	0.001	0.080	-0.025	-0.328	-0.170	-0.242
	(-0.255)	(-0.406)	(-0.330)	(-0.009)	(0.075)	(-0.029)	(-0.305)	(-0.133)	(-0.232)
CH_3O-6O	-0.210	-0.349	-0.303	0.000	0.082	-0.024	-0.340	-0.184	-0.253
	(-0.236)	(-0.394)	(-0.318)	(-0.009)	(0.078)	(-0.026)	(-0.325)	(-0.148)	(-0.244)
CH_3O-7	-0.252	-0.359	-0.328	-0.006	0.077	-0.026	-0.289	-0.173	-0.230
	(-0.282)	(-0.402)	(-0.343)	(-0.015)	(0.074)	(-0.029)	(-0.273)	(-0.138)	(-0.220)
CH_3-5	-0.255	-0.365	-0.336	0.008	0.086	-0.014	-0.285	-0.161	-0.219
	(-0.287)	(-0.407)	(-0.355)	(-0.001)	(0.083)	(-0.016)	(-0.267)	(-0.124)	(-0.206)
H-4	-0.247	-0.352	-0.308	0.016	0.095	-0.009	-0.297	-0.174	-0.244
	(-0.277)	(-0.405)	(-0.329)	(0.007)	(0.094)	(-0.010)	(-0.284)	(-0.131)	(-0.234)
H-5	-0.257	-0.364	-0.338	0.011	0.087	-0.011	-0.281	-0.160	-0.216
	(-0.289)	(-0.405)	(-0.357)	(0.002)	(0.084)	(-0.013)	(-0.262)	(-0.122)	(-0.203)
H-6	-0.233	-0.352	-0.320	0.011	0.082	-0.016	-0.302	-0.167	-0.232
	(-0.271)	(-0.395)	(-0.338)	(0.002)	(0.077)	(-0.018)	(-0.278)	(-0.130)	(-0.220)
H-6O	-0.220	-0.342	-0.315	0.013	0.083	-0.014	-0.316	-0.180	-0.238
	(-0.250)	(-0.380)	(-0.327)	(0.004)	(0.080)	(-0.015)	(-0.297)	(-0.146)	(-0.231)
H-7	-0.256	-0.352	-0.332	0.002	0.079	-0.017	-0.278	-0.169	-0.222
	(-0.263)	(-0.392)	(-0.348)	(0.002)	(0.077)	(-0.020)	(-0.271)	(-0.134)	(-0.211)
Cl-4	-0.250	-0.358	-0.312	0.021	0.101	-0.006	-0.293	-0.163	-0.236
	(-0.281)	(-0.404)	(-0.334)	(0.012)	(0.099)	(-0.006)	(-0.278)	(-0.123)	(-0.224)
CF_3-4	-0.253	-0.351	-0.318	0.026	0.104	0.000	-0.286	-0.158	-0.228
	(-0.283)	(-0.392)	(-0.342)	(0.017)	(0.102)	(0.001)	(-0.271)	(-0.118)	(-0.213)
CF_3-5	-0.262	-0.356	-0.344	0.020	0.094	-0.003	-0.268	-0.147	-0.203
	(-0.293)	(-0.390)	(-0.362)	(0.012)	(0.091)	(-0.004)	(-0.249)	(-0.110)	(-0.188)

[a]DMSO values given in parentheses. [b]Transition state structure.

of the *TS* structure. Figure 3, on the other hand, also illustrates the influence of N-heterocycle on $\Delta G^{\ddagger}$; for any given reaction medium, $\Delta G^{\ddagger}$ diminishes in the order X-4 > X-5 > X-6O > X-6 ≈ X-7. Such a trend is interpreted in terms of the ability of $N^{(3)}$ to donate electrons (and ultimately, to stabilize a positive charge at the zwitterionic *TS* structure). For cyclic amines, the intrinsic electron-donating ability of N (evaluated by the reactive hybrid orbital theory) is shown to increase in the order azetidine < pyrrolidine < piperidine [11], and reported vertical ionization potentials decrease in the order azetidine > pyrrolidine > piperidine ≈ azepine [12]. These findings reveal an increase in electron-donating ability of N with increasing ring size, and are rationalized in terms of the change in hybridization of the N atom, i.e., as the ring size increases the s-character of the N nonbonding orbital decreases [11], hence the lone pair electrons are held less tightly. The noticeable

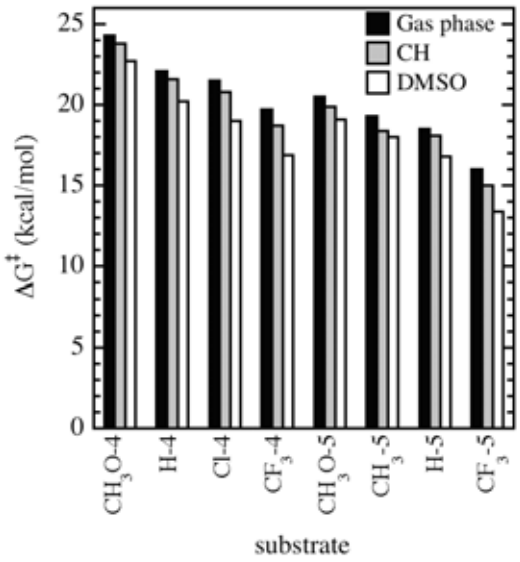

Figure 2. Calculated Gibbs energies of activation for isomerization (at 21°C) of azetidine (X-4) and pyrrolidine (X-5) derivatives.

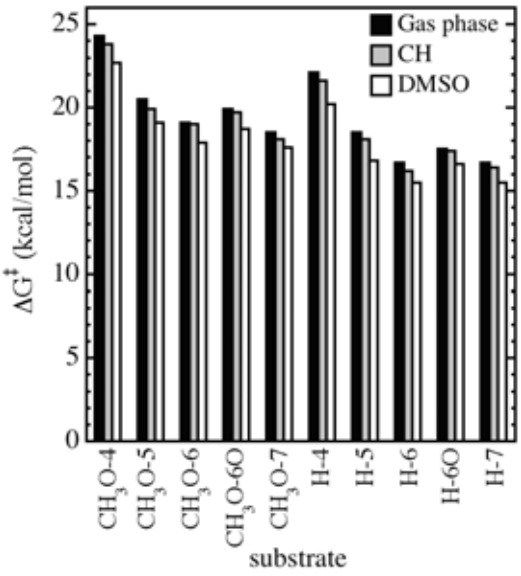

Figure 3. Calculated Gibbs energies of activation for isomerization (at 21°C) of CH_3O and H series.

decrease in reactivity on going from X-6 to X-6O, on the other hand, is attributed to a lower $N^{(3)}$ electron-donating ability due to the inductively withdrawing (-I) effect of oxygen.

Trends described above for computed $\Delta G^{\ddagger}$ values agree well with experimental reactivity trends, as

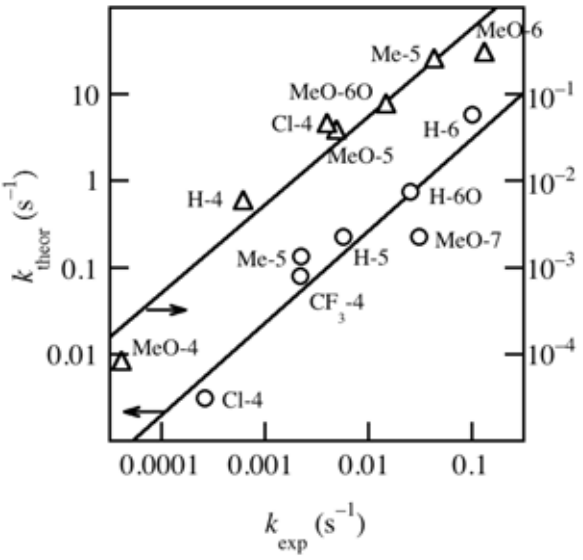

Figure 4. Plot of calculated rate constants (k_{theor}) for isomerization in cyclohexane (O) or DMSO (Δ) vs. experimental values (k_{exp}, taken from ref. [3]).

illustrated in Figure 4, in which calculated rate constants for isomerization in CH and DMSO (obtained by using Eyring transition state theory [13] and computed $\Delta G^{\ddagger}$ values presented in Figures 2 and 3) are plotted against reported experimental rate constants (determined at 21°C, [3]); resulting slope values are (1.1 ± 0.2) and (1.0 ± 0.1) for CH and DMSO, respectively. Although computed $\Delta G^{\ddagger}$ values reproduce *qualitatively* experimental trends, it is also evident from Figure 4 that computed Gibbs energies of activation are somewhat underestimated, since calculated rate constants in CH are ca. 7 to 57 times, and those calculated in DMSO are ca. 2 to 12 times, higher than the experimental values; these ratios would correspond to an underestimate of $\Delta G^{\ddagger}$ ranging from ca. 2% to 13%. It is worthy to note that underestimation of DFT computed Gibbs energies of activation has recently been reported as well for thermal *cis*-to-*trans* isomerization of azobenzenes [14] and aromatic imines [15], for example. Nevertheless, since theoretical rate constants increase by essentially the same order of magnitude as the experimental ones when varying solvent or structure, relative rates for thermal *cis*-to-*trans* isomerization of 1-phenyltriazenes derived from cyclic amines can be predicted reasonably well.

In summary, DFT calculations at the B3LYP/6-31G(d) level of theory, with solvents modeled as a polarizable continuum, predict that thermal *cis*-to-*trans* isomerization of N-(phenylazo)-substituted nitrogen heterocycles proceeds by a rotation mechanism via a zwitterionic transition state form. Valuable insights into the structure of ground-state species are also revealed. Computed Gibbs energies of activation reproduce qualitatively well the reactivity trends determined experimentally on varying phenyl substituent, N-heterocycle, and solvent. The ability to computationally predict the (relative) influence of substituents and reaction medium on the lifetime of *cis* isomers should prove advantageous for the customized design of photo-responsive N-(phenylazo)-substituted nitrogen heterocycles for specific applications.

ACKNOWLEDGMENTS

This work was made possible by the facilities of the Shared Hierarchical Academic Research Computing Network (SHARCNET) and Compute/ Calcul Canada.

REFERENCES

1. (a) Dugave, C. and Demange, L. 2003, Chem. Rev., 103, 2475. (b) Altoè, P., Bernardi, F., Conti, I., Garavelli, M., Negri, F. and Orlandi, G. 2007, Theor. Chem. Acc., 117, 1041. (c) Russew, M-M. and Hecht, S. 2010, Adv. Mater., 22, 3348. (d) Natali, M. and Giordani, S. 2012, Chem. Soc. Rev., 41, 4010.
2. Zhao, P., Zhang, Z., Wang, P. J. and Liu, D. S. 2009, Physica. B, 404, 3462.
3. Fu, J., Lau, K. and Barra, M. 2009, J. Org. Chem., 74, 1770.
4. Tabone, R. and Barra, M. 2011, Dyes Pigm., 88, 180.
5. Bandara, H. M. D. and Burdette, S. C. 2012, Chem. Soc. Rev., 41, 1809, and references therein.
6. Frisch, M. J., Trucks, G. W., Schlegel, H. B., Scuseria, G. E., Robb, M. A., Cheeseman, J. R., Scalmani, G., Barone, V., Mennucci, B., Petersson, G. A., Nakatsuji, H., Caricato, M., Li, X., Hratchian, H. P., Izmaylov, A. F., Bloino, J., Zheng, G., Sonnenberg, J. L., Hada, M., Ehara, M., Toyota, K., Fukuda, R., Hasegawa, J., Ishida, M., Nakajima, T., Honda, Y., Kitao, O., Nakai, H., Vreven, T., Montgomery, J. A. Jr., Peralta, J. E., Ogliaro, F., Bearpark, M., Heyd, J. J., Brothers, E., Kudin, K. N., Staroverov, V. N., Keith, T., Kobayashi, R., Normand, J., Raghavachari, K., Rendell, A., Burant, J. C., Iyengar, S. S., Tomasi, J., Cossi, M., Rega, N., Millam, J. M., Klene, M., Knox, J. E., Cross, J. B., Bakken, V., Adamo, C., Jaramillo, J., Gomperts, R., Stratmann, R. E., Yazyev, O., Austin, A. J., Cammi, R., Pomelli, C., Ochterski, J. W., Martin, R. L., Morokuma, K., Zakrzewski V. G., Voth, G. A., Salvador, P., Dannenberg, J. J., Dapprich, S., Daniels, A. D., Farkas, O., Foresman, J. B., Ortiz, J. V., Cioslowski, J. and Fox, D. J. 2010, Gaussian 09, Revision C.01; Gaussian, Inc., Wallingford.
7. Tomasi, J., Mennucci, B. and Cancès, E. 1999, J. Mol. Struct., 464, 211.
8. Fu, J. 2008, M.Sc. thesis, University of Waterloo.
9. Wang, C-K., Wang, Y-H., Su, Y. and Luo, Y. 2003, J. Chem. Phys., 119, 4409.
10. Reichardt, C. 2003, Solvents and Solvent Effects in Organic Chemistry, Wiley-VCH, Weinheim, Ch. 5.
11. Ohwada, T., Hirao, H. and Ogawa, A. 2004, J. Org. Chem., 69, 7486.
12. Yoshikawa, K., Hashimoto, M. and Morishima, I. 1974, J. Am. Chem. Soc., 96, 288.
13. Eyring, H. 1935, Chem. Rev., 17, 65.
14. Wazzan, N. A., Richardson, P. R. and Jones, A. C. 2010, Photochem. Photobiol. Sci., 9, 968.
15. Luo, Y., Utecht, M., Dokić, J., Korchak, S., Vieth, H-M., Haag, R. and Saalfrank, P. 2011, Chem. Phys. Chem., 12, 2311.